Nyquist-filtering (De)multiplexer Using a Ring Resonator Assisted Interferometer Circuit

Leimeng Zhuang, Chen Zhu, Yiwei Xie, Maurizio Burla, Chris G. H. Roeloffzen, Marcel Hoekman, Bill Corcoran and Arthur J. Lowery

***Abstract*—We present an optical Nyquist-filtering (de)multiplexer using a ring resonator assisted interferometer circuit. It features a near-rectangular passband shape, scalable port count, and can be designed with sub-GHz spectral resolution. The circuit can be constructed using ordinary passive photonic integrated circuit building blocks. In contrast to its counterparts using tapped-delay-line circuit topologies, this requires two-orders-of-magnitude smaller chip area and easier control. The results of this work show the potential for realizing high-spectral-efficiency multi-carrier transceivers and reconfigurable optical add-drop multiplexers in a fully-integrated form.**

***Index Terms*—Nyquist filter, multiplexing, WDM, optical signal processing, photonic integrated circuit, waveguide device, discrete Fourier transform, fiber communications, transceiver.**

I. Introduction

MULTI-CARRIER techniques, such as super-channels and Nyquist wavelength division multiplexing (N-WDM) are of great interest for next-generation high-capacity, elastic optical communication networks [1, 2], as they support high spectrum utilization by allowing carriers to be spaced at or close to signal baud rate. N-WDM is in particular promising for flexible channel management as it allows Nyquist channel shaping and (de)multiplexing functions to be implemented by means of optical filters [3–5], which reduces the power-consuming workload of digital signal processing in the system and avoids the associated processing latency as well as signal conversions between the optical and electrical domain. For multi-carrier transceiver applications, optical (de)multiplexers that are suitable for N-WDM systems and are able to shape the transmitted spectra to be only slightly wider than the signal baud rate, namely Nyquist-filtering (de)multiplexers, are a highly desired function. Combining Nyquist filtering and (de)multiplexing in one device not only brings benefits to transceiver complexity and overall loss, but also provides a useful building block for constructing reconfigurable optical add-drop multiplexers (ROADMs) [6–8] for N-WDM-based networks that have great application potential for the future optical communication technologies.

To date, a number of studies of Nyquist-filtering (de)multiplexers have been reported. Conventional implementations using free-space optics have demonstrated great flexibility regarding filter passband characteristics; however, these have a common trade-off between spectral resolution and device complexity [3–5]. Alternatively, photonic integrated circuit (PIC)-based implementations offer several desirable features, i.e. significant reduction of device size, potential for low-cost fabrication, and simple packaging processes [9–12]. In terms of the circuit configuration, an arrayed-waveguide grating (AWG) with a synchronized Mach-Zehnder interferometer (MZI) is a widely investigated (de)multiplexer featuring a flat-top passband [13, 14]. However, due to the intrinsic diffraction in the slab waveguide [15], the outer ports of the (de)multiplexer suffer from higher loss and frequency deviation relative to the inner ports. An effective solution for this issue is to replace the AWG by a discrete Fourier transform (DFT) circuit based on a matrix of couplers, phase shifts, and delay lines [16]. When a DFT circuit is combined with additional processing stages, a Nyquist-filtering (de)multiplexer can be devised with custom passband shaping according to various application requirements [17, 18]. Although these designs have been successfully demonstrated, all the (de)multiplexer demonstrations to date are based on tapped-delay-line circuit topologies (characterized by a finite impulse response (FIR) in terms of signal processing), which have, in general, a trade-off between filtering performance and circuit complexity. For the purpose of Nyquist-filtering, such circuit topologies need a significant number of delay lines with a maximum length of >10× the unit delay (which determines the circuit free spectral range (FSR) [19]) to achieve sharp passband transition and sufficient stopband extinction. However, a near-rectangular passband accompanied by a stopband extinction > 35 dB, is highly desired to minimize the inter-sub-carrier/inter-channel crosstalk, which is a key performance metric that determines the practicality of the device. For example, a circuit implementing a raised cosine filter with an excess bandwidth of 2% of the ideal Nyquist bandwidth will require more than a hundred taps, implying an impractical number of delay lines with a maximum delay equal to the product of the tap number and the unit delay [20–22]. In terms of device fabrication, such a complex circuit requires a large chip area and therefore bears high risk of waveguide quality non-uniformity across the chip and high sensitivity for circuit parameter errors due to fabrication tolerance, which may lead to severe performance degradation and low device yield.

Issue No xxxxxxxxxxxxx 2015.

This work was supported in part by the Australian Research Council Laureate fellowship with grant no. FL13010041.

Dr. Leimeng Zhuang, Dr. Chen Zhu, Yiwei Xie, Dr. Bill Corcoran, and Prof. Arthur J. Lowery is with the Electro-Photonics Laboratory, Department of Electrical and Computer Systems Engineering, Monash University, Australia (Leimeng.zhuang@monash.edu). B. Corcoran and A. J. Lowery are also with the Centre for Ultrahigh-bandwidth Devices for Optical Systems (CUDOS), Australia.

Dr. Maurizio Burla is with the Institut National de la Recherche Scientifique (INRS-EMT), Montréal, Canada.

Dr. Chris G. H. Roeloffzen and Mr. Marcel Hoekman are with the SATRAX B.V. and LioniX B.V., The Netherlands.

In this work, we present a novel PIC implementation of an optical Nyquist-filtering (de)multiplexer that breaks the aforementioned trade-off between filtering performance and circuit complexity. It features a near-rectangular passband, scalable port count, and can be designed with sub-GHz spectral resolution. This unique combination of merits is provided by a ring resonator-assisted interferometer circuit incorporating discrete Fourier transform function (RADFT), which can be constructed using ordinary passive PIC building blocks [19]. Our circuit solution uses a maximum of three ring resonators to perform the Nyquist passband shaping with a minimum excess bandwidth (defined the band's edge to the -25-dB stop-band) of 2% of the ideal Nyquist bandwidth. This excess bandwidth is an order-of-magnitude smaller than a recently reported solution based on a tapped-delay-line topology that would require a two-orders-of-magnitude larger circuit to provide a comparable passband shape [18]. We also present a proof-of-concept experiment of optical generation of Nyquist-spacing super-channel and the transmission of the generated signal using a demonstrator chip comprising a two ring resonator-assisted asymmetric Mach-Zehnder interferometer (2RAMZI) [23–25], equivalent to a 2-port RADFT as explained in this work. The results of this work show potential for realizing high-spectral-efficiency multi-carrier transceivers and ROADMs in a fully-integrated form.

The remainder of the paper is organized as follows: Section 2 explains the device principle; Section 3 and 4 show, respectively, a simulation and an experiment of optical generation of a Nyquist-spacing super-channel using a RADFT circuit; and Section 5 provides the conclusion.

II. Device Principle

Figure 1 shows the signal processing principle of the proposed device. It comprises three sections, i.e. a $N \times N$ DFT operation, an array of delay lines incorporated in a $N \times 2$ combining operation, and a 2×1 combining with each input processed by an infinite impulse response (IIR) filter. In terms of signal processing, this is a time-invariant moving-average auto-regressive system, and its frequency response characteristics can be derived from an equivalent digital filter model, using z-transform [19]. Accordingly, the transfer functions between the inputs and positions (i) and (ii) in Fig. 1 are given by

$$H_i^{(\mathrm{i})}(z) = \sum_{g=0}^{N/2-1} e^{-\mathrm{j}2\pi i \cdot g/N} \cdot z^{-g} \quad (1)$$

$$H_i^{(\mathrm{ii})}(z) = \sum_{g=N/2-1}^{N-1} e^{-\mathrm{j}2\pi i \cdot g/N} \cdot z^{-g} \quad (2)$$

where $z = r \cdot \exp(-\mathrm{j}2\pi f \cdot \Delta\tau)$ with $r = [0, 1]$ denoting the amplitude attenuation due to the signal propagation loss, f the frequency, and $\Delta\tau$ the unit delay that determines the device free spectral range (FSR) by $f_{\mathrm{FSR}} = 1/\Delta\tau$. The transfer function of the IIR filter is given by

$$H_{\mathrm{IIR}}(z) = \sum_{m=1}^{M} \frac{\sqrt{1-\kappa_m} - e^{-\mathrm{j}\phi_m} \cdot z^{-N}}{1 - e^{-\mathrm{j}\phi_m} \cdot z^{-N} \cdot \sqrt{1-\kappa_m}} \quad (3)$$

Combining Eq. (1) – (3), the complete transfer function from the inputs to the output at position (v) is

$$\begin{aligned} H_i(z) &= H_i^{(\mathrm{iii})}(z) + H_i^{(\mathrm{iv})}(z) \\ &= H_i^{(\mathrm{i})}(z) H_{\mathrm{IIR}}^{(\mathrm{iii})}(z) + H_i^{(\mathrm{ii})}(z) H_{\mathrm{IIR}}^{(\mathrm{iv})}(z) \\ &= \Big(\sum_{g=1}^{N/2-1} e^{-\mathrm{j}2\pi i \cdot g/N} \cdot z^{-g}\Big) \cdot \Big(\sum_{p=1}^{P} \frac{\sqrt{1-\kappa_p} - e^{-\mathrm{j}\phi_p} \cdot z^{-N}}{1 - e^{-\mathrm{j}\phi_p} \cdot z^{-N} \cdot \sqrt{1-\kappa_p}}\Big) + \\ &\quad \Big(\sum_{g=N/2}^{N-1} e^{-\mathrm{j}2\pi i \cdot g/N} \cdot z^{-g}\Big) \cdot \Big(\sum_{q=1}^{Q} \frac{\sqrt{1-\kappa_q} - e^{-\mathrm{j}\phi_q} \cdot z^{-N}}{1 - e^{-\mathrm{j}\phi_q} \cdot z^{-N} \cdot \sqrt{1-\kappa_q}}\Big) \end{aligned} \quad (4)$$

For waveguide implementation, when $N = 2^n$ with n an integer, the first and second sections can be merged together

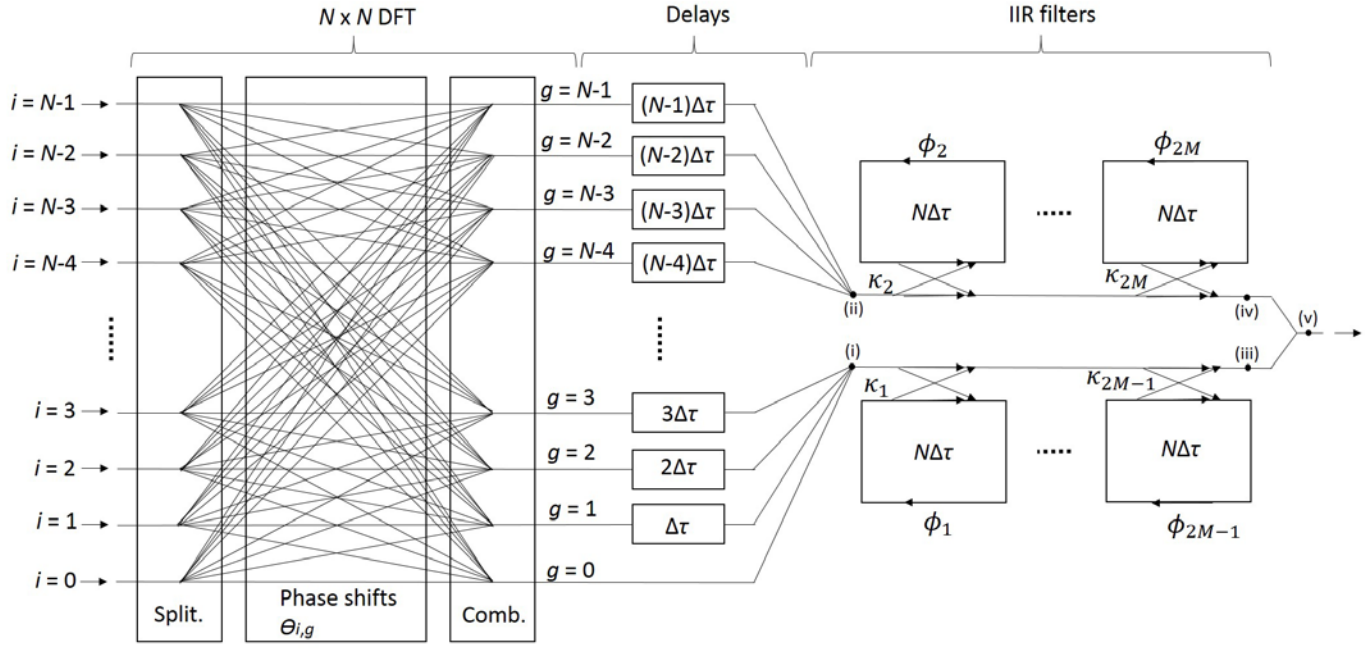

Fig. 1. Illustration of signal processing principle of a N-port RADFT.

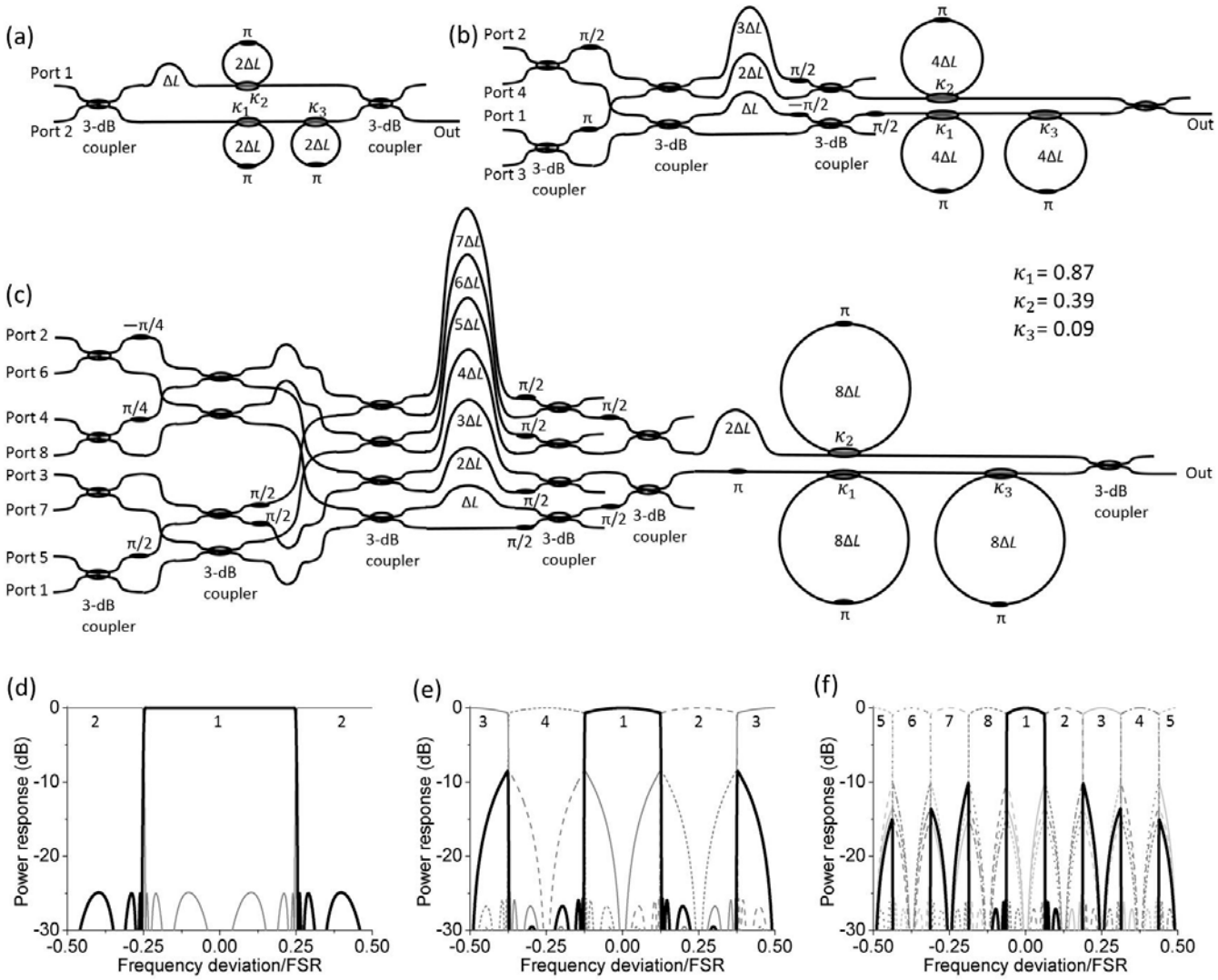

Fig. 2. (a-c) schematics of RADFT circuits with 2, 4, and 8 ports, (d-f).corresponding channel frequency responses.

and implemented using a DFT circuit topology as explained in [16]. The IIR filters can be implemented using side-coupled ring resonators [10]. As examples, Fig. 2a to 2c depict the schematics of three RADFT circuits with N equal to 2, 4, and 8, respectively. Here, a waveguide length of ΔL produces a unit time delay $\Delta\tau = \Delta L \cdot n_g/c_0$ with n_g the group index of the waveguide and c_0 the speed of light in vacuum [19]. The corresponding (de)multiplexer frequency responses are depicted in Fig. 2d to 2f, showing near-rectangular passbands for different input ports, with a frequency spacing equal to the -3-dB passband bandwidth. To give a straightforward understanding how the passbands are synthesized, Fig. 3 provides a frequency-domain illustration of the device principle based on 'Port 1' of the 4-port RADFT, where signal propagation loss is assumed to be small ($r \approx 1$), and so has a negligible effect on the frequency response. Referring to the position (i) and (ii) in Fig. 1, the frequency responses from the 4 × 2 DFT operation are depicted in Fig. 3a, showing identical amplitude factors and linear phase shifts with a slope difference of $(N/2 = 2)\Delta\tau$. The vector combining of these results in the frequency response shown in Fig. 3b, corresponding to an ordinary 4 × 1 DFT operation. Referring to positions (iii) and (iv) in Fig. 1, the IIR filters work as all-pass filters [19] and introduce a modification to the phase shifts as shown in Fig. 3c. With the parameter κ and ϕ values as indicated in Fig. 2, an in-phase regime (phase difference of 2π) is created around the center of the DFT passband, neighbored by anti-phase regimes (phase difference of $2\pi \pm \pi$), with narrow transitions in-between. As the result of this, the frequency response at the output features a near-rectangular passband with a stopband extinction of 25 dB and sharp transition bands as shown in Fig. 3d. Basically, the transition band sharpness is governed by the number of ring resonators.

Figure 4 depicts the optimized passbands when using 1, 2, and 3 ring resonators. The 3-ring configuration features a -25-dB excess bandwidth as small as 2% of the -3-dB bandwidth, or in other words, a passband-to-stopband transition equal to 1% of the -3-dB bandwidth. This means that one can design a -3-dB bandwidth up to 100 GHz with the transition spanning less than 1 GHz, corresponding to filter frequency selectivity at sub-GHz spectral resolution. In terms of N-WDM multiplexing, such a passband shape will allow for very dense

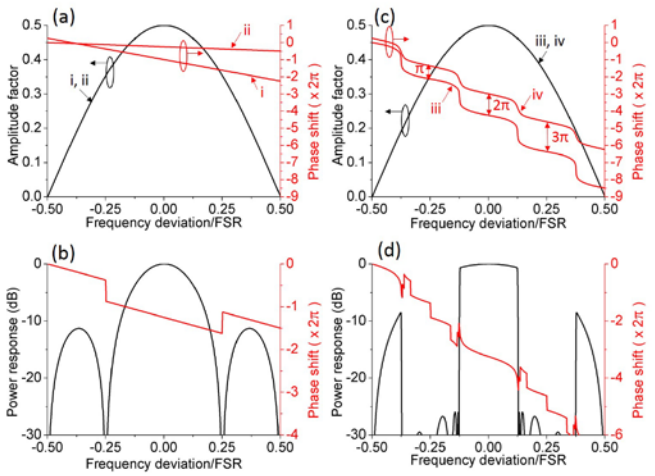

Fig. 3. Frequency-domain illustration of device principle based on 'Port 1' of the 4-port RADFT: (a) frequency responses at position (i) and (ii) in Fig. 1, (b) the corresponding frequency response by vector-combining of (i) and (ii); (c) frequency responses at position (iii) and (iv) in Fig. 1, (d) the corresponding frequency response by vector-combining of (iii) and (iv).

multiplexing, e.g. Nyquist-spacing multiplexing. In principle, further sharpening of the transition bands is still possible by increasing the number of ring resonators. However, in practice, this means that the added ring resonators must operate with κ values approaching zero, corresponding to high-Q resonance status [26], which raises challenges with respect to performance sensitivity to fabrication tolerance and control accuracy. In case some applications require a (de)multiplexing function with a higher stopband extinction (e.g. > 35 dB), a possible solution is to cascade an additional filter to each of the N ports of the initial (de)multiplexer, e.g. using the interleaver as in Fig. 2a which should be designed with the same passband bandwidth as the initial (de)multiplexer. Figure 4 also depicts the passband dispersion and the effect of loss. When applied for Nyquist filtering/shaping, these two properties of the device will distort the transmitted signals away from the ideal Nyquist pulse shape, causing inter-symbol interference. However, these are linear distortions, so a compensation can be applied at the digital receiver by means of equalization techniques [27].

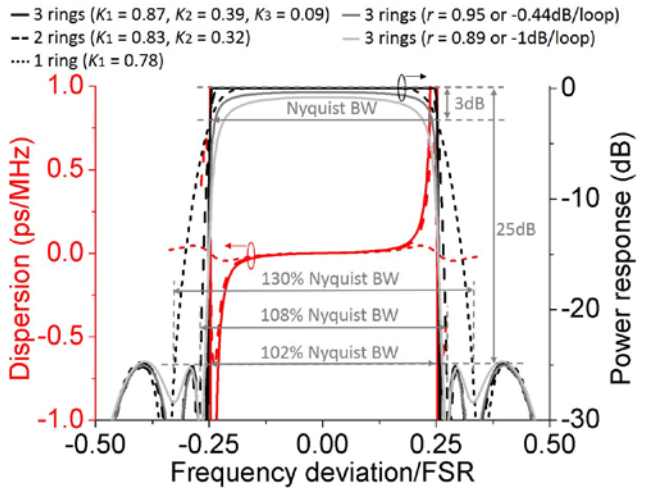

Fig. 4. Passband characteristics when having different number of ring resonators and different values of loss (calculated from the 2-port RADFT).

III. SIMULATION OF TRANSMISSION

Figure 5 shows a simulation of Nyquist-spacing super-channel generation and transmission, using 8-port RADFTs (see Fig. 2d) as transmitter Nyquist-filtering multiplexer and receiver super-channel demultiplexer. Here, we considered a 7-sub-carrier scenario, where the sub-carriers are QPSK-modulated at a symbol rate of 20 Gbaud, consistent with the (de)multiplexer -3-dB-passband bandwidth. Figure 5b depicts the spectrum of a single sub-carrier at the output of the multiplexer, showing reduced signal bandwidth as the result of Nyquist filtering. When 7 sub-carriers are operating simultaneously, a Nyquist-spacing super-channel is generated, with its spectrum as shown in Fig. 5c. Figure 5d depicts the spectrum of one demultiplexed sub-carrier at one demultiplexer output. The demultiplexed sub-carrier is then passed through a 40-GHz-bandwidth Gaussian filter to remove the residual sidelobes coming from the other sub-carriers, and is subsequently sent to a digital coherent receiver for optimal reception. Figure 5e depicts the system back-to-back (B2B) performance in signal quality factor (Q) versus 0.1-nm-resolution optical signal-to-noise ratio (OSNR), showing the viability of such a system. Here, the system performances are compared for RADFTs with different number of ring resonators. When using more ring resonators, we expect the decreased inter-sub-carrier crosstalk to improve the system performance, which is manifested by the OSNR at error-free threshold for 7% forward error correction (7%FEC, corresponding to Q = 8.53), namely OSNR of 10 dB, 9.5 dB, and 8.5 dB for using 1, 2, and 3 ring resonators, respectively.

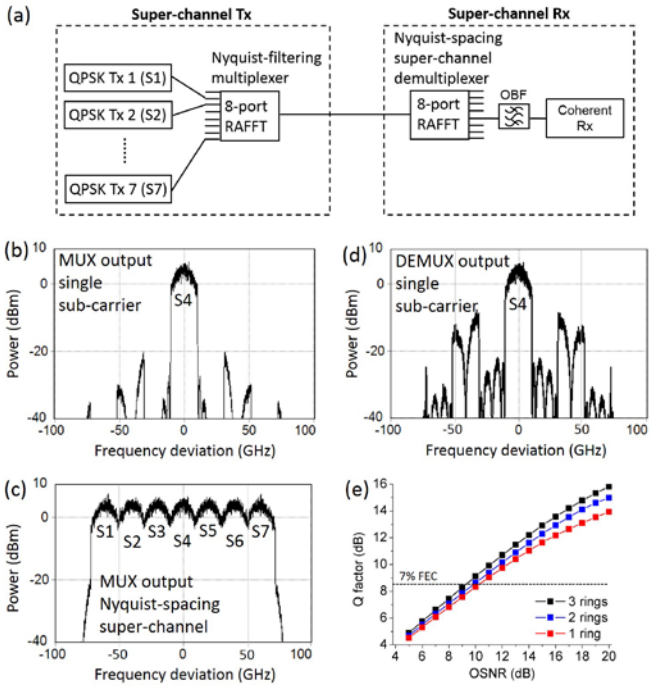

Fig. 5. Simulation of Nyquist-spacing super-channel generation and transmission, using 8-port RADFTs as transmitter Nyquist-filtering multiplexer and receiver super-channel demultiplexer: (a) transmission system configuration, (b) multiplexer output spectrum of a single sub-carrier, (c) multiplexer output spectrum of a 7-sub-carriers super-channel, (d) spectrum of a demultiplexed sub-carrier, (e) system B2B performance in Q vs OSNR.

IV. Experimental Demonstration

In this section, we show a proof-of-concept experiment for optical generation of a Nyquist-spaced super-channel using a 2-port RADFT circuit employing 2 ring resonators, namely a 2RAMZI interleaver [23–25]. The circuit is designed with a FSR of 25 GHz and is equipped with circuit parameter reconfigurability using a thermo-optical tuning mechanism. The chip is fabricated in a commercial low-loss, high-index-contrast Si_3N_4 waveguide technology (TriPleX [28, 29]), with the total fiber-to-fiber insertion loss of the chip measured to be 9 dB, which is dominated by two times fiber-chip coupling losses about 4 dB/facet (however, this is expected to decrease significantly when the design of waveguide facet or interposer is optimized for fiber-chip coupling). The complete experiment setup is illustrated in Fig. 6. Here, two-data-stream interleaving scheme is used for simplicity, where 6 equal-power CW lasers with a constant frequency interval of 25 GHz are used to generate the odd sub-carriers, and a 12.5-GHz serrodyne frequency shifter [30] is employed to generate the even sub-carriers. The sub-carriers are QPSK modulated at 12.5 Gbaud, with odd and even sub-carriers decorrelated by means of a time delay difference prior to the 2RAMZI interleaver. Figure 7a depicts the measured passband characteristics of the 2RAMZI interleaver, showing good agreement with theory. We show an 8% excess bandwidth slightly smaller than 1-GHz, demonstrating that these filters can provide sub-GHz resolution. Figure 7b shows the interleaver function with both bar-port and cross-port frequency responses depicted. The close filter shape resemblance between the two ports and frequency periodicity of the passbands indicate good waveguide uniformity and design accuracy of the device. As the waveguides are designed for optimal coupling to the TE-polarization of the chip, polarization management is conducted throughout our experiment setup. With the sub-carriers frequency-aligned with the interleaver passbands, a 12 × 12.5 Gbaud Nyquist-spacing super-channel is generated at the output of the interleaver. Figure 7c and 7d depict the output spectra of a single sub-carrier and the 12-sub-carrier super-channel, respectively. As can be seen in single sub-carrier case, the modulated QPSK spectrum has a portion of its sidelobes falling in the neighboring passbands of the interleaver, leading to inter-sub-carrier interference. However, in the case of RADFT circuits with 4 or more input ports, this sidelobe issue will be avoided owing to sufficient suppression at the sidelobe frequencies (Fig. 5b). To remove these residual sidelobes, one way is to add optical pre-filtering prior to the interleaver as explained in [31, 32]. In our experiment, however, we implemented equivalent pre-filtering in the digital domain before modulation, in accordance with the equipment availability.

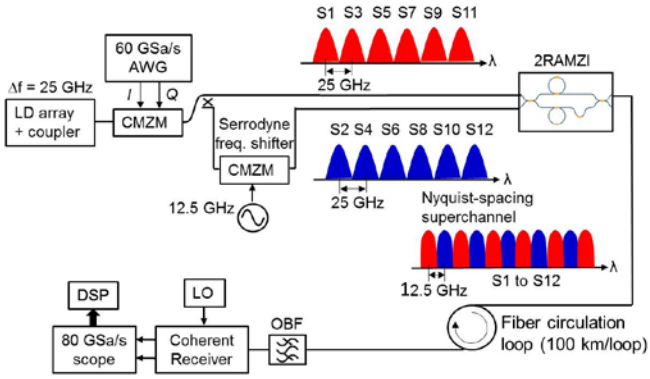

Fig. 6. Experiment setup for optical generation of Nyquist-spacing super-channel using a 2RAMZI interleaver.

Further, we performed transmission experiments with the generated super-channel to verify the viability of the proposed approach. The signal was sent into a fiber re-circulation loop consisting of a single 100-km long, SSMF span, with EDFA-only amplification. The sub-carrier in the middle, 'S7', was coherently received, where the digital receiver uses a single-polarization constant modulus algorithm to converge to matched filter solution [33], followed by differential Viterbi-Viterbi frequency offset estimation and Viterbi-Viterbi phase estimation algorithms to recover the signals [34]. Figure 8a depicts signal *Q* versus transmission distance, which shows a successful transmission over 4000 km with the *Q* above 8.53 (7% FEC threshold). Figure 8b shows the optimal launch power for 4000-km transmission. It can be seen that when the launch power is larger than 5 dBm, *Q* degrades due to nonlinear effects in the fiber. For comparison, in Fig. 8a and 8b, we also show in the transmission of a similar super-channel with the Nyquist-filtering of the sub-carriers performed before modulation using 0.08-roll-off digital RRC filtering instead of our 2RAMZI interleaver. These results verify the viability of our optical super-channel generation approach and prove that the 2RAMZI interleaver is able to perform an equivalent Nyquist-filtering function to their digital counterparts with similar transition band characteristics. Figure 8c shows the 4000-km transmission of the super-channels generated using different frequency regimes of the 2RAMZI interleaver chip (configured with a fixed setting of circuit parameters), ranging from 191.5 THz to 196 THz. The resulting *Q* variation is about 0.8 dB. This demonstration shows that the proposed Nyquist-filtering (de)multiplexers is able to be implemented with full-C-band

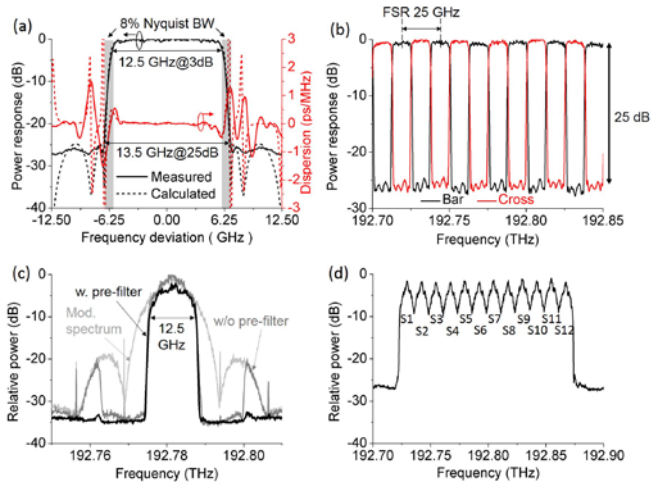

Fig. 7. (a) Measured 2RAMZI passband characterisitcs, (b) demonstration of interleaver function, (c) output spectrum of a single sub-carrier, (d) output spectrum of the generated Nyquist-spacing super-channel.

coverage. For various system applications, this feature can be utilized to offer benefits in terms of system complexity, power-consumption, and construction cost.

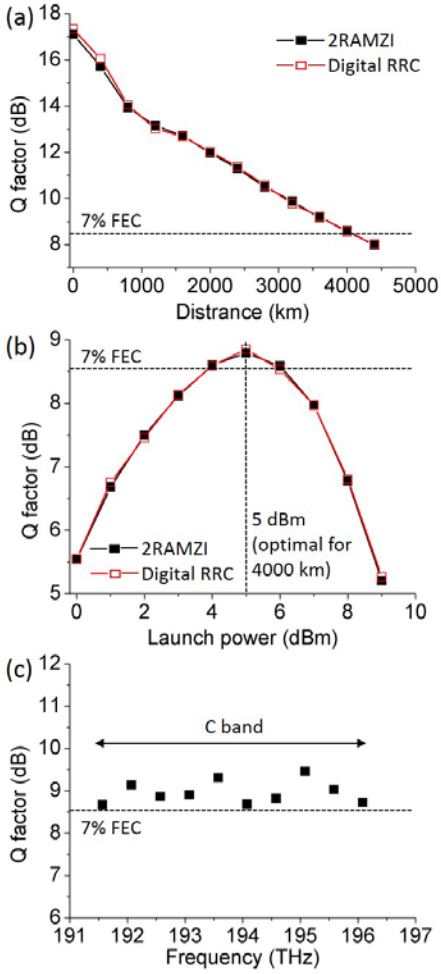

Fig. 8. (a) Super-channel transmission versus distance, (b) optimal launch power for 4000 km, (c) 4000-km transmission of super-channels generated using different frequency regimes of the 2RAMZI interleaver chip.

V. Conclusions

The proposed N-port RADFT circuits are able to provide near-rectangular passbands for different input ports at a spacing equal to the -3-dB bandwidth. This function can be used to perform optical Nyquist filtering and dense multiplexing with small inter-channel crosstalk. The experimental demonstration of optical generation of a Nyquist-spaced super-channel using a 2RAMZI interleaver chip verifies the function of the proposed circuits and shows that it provides not only an equivalent performance as its digital filter counterpart using similar transition band sharpness, but also can be implemented with an operating frequency range covering the entire C band. The results of this work show potential for realizing high-spectral-efficiency multi-carrier transceivers and ROADMs in a fully-integrated form.

References

[1] Gerstal, O., Jino, M., Lord, A., Yoo, S. J. B., "Elastic Optical Networking: A New Design Dawn for the Optical Layer?," IEEE Communication Magazine, P. S12, (2012).

[2] Yin, Y., Wen, K., Geisler, D. J., Liu, R., and Yoo, S. J. B., "Dynamic on-demand defragmentation in flexible bandwidth elastic optical networks," Opt. Express, vol. 20, no. 2, 1798-1804 (2012).

[3] Ziyadi, M., Chitgarha, M. R., Mohajerin-Ariaei, A., Khaleghi, S., Almaiman, A., Cao, Y., Willner, M. J., Tur, M., Paraschis, L., Langrock, C., Fejer, M. M., Touch, J. D., and Willner, A. E., "Optical Nyquist channel generation using a comb-based tunable optical tapped-delay-line," Opt. Lett., vol. 39, no. 23, 6585-6588 (2014).

[4] Roelens, M. A. F., Frisken, S., Bolger, J. A., Abakoumov, D., Baxter, G., Poole, S., and Eggleton, B. J., "Dispersion Trimming in a Reconfigurable Wavelength Selective Switch," J. Lightwave Technol., vol. 26, no. 1, 73-78 (2008).

[5] Rudnick, R., Tolmachev, A., Sinefeld, D., Golani, O., Ben-Ezra, S., Nazarathy, M., and Marom, D. M., "Sub-Banded/Single-Sub-Carrier Drop-Demux and Flexible Spectral Shaping with a Fine Resolution Photonic Processor," European Conference on Optical Communications (ECOC2014), PD. 4.1.

[6] Frisken, S., Baxter, G., Abakoumov, D., Zhou, H., Clarke, I., and Poole, S., "Flexible and Grid-less Wavelength Selective Switch using LCOS Technology," Proc. OFC2011, OTuM3, 2011, LA.

[7] Sakamaki, Y., Kawai, T., Komukai, T., Fukutoku, M., Kataoka, T., Watanabe, T., and Ishii, Y., "Experimental Demonstration of Multi-degree Colorless, Directionless, Contentionless ROADM for 127-Gbit/s PDM-QPSK Transmission System," Opt. Express, vol. 19, no. 26, B1-11, 2011.

[8] Cho, J. S., Seo, Y. K., Yoo, H., Park, P. K. J., Rhee, J. K., Won, Y. H., and Kang, M. H., "Optical burst add-drop multiplexing technique for sub-wavelength granularity in wavelength multiplexed ring netoworks," Opt. Express, 15(20), 13256-13265 (2007).

[9] Smit, M., van der Tol, J. & Hill, M., Moore's law in photonics. *Laser & Photo. Rev.* **6,** 1-13 (2012).

[10] Roeloffzen, C. G. H., Zhuang, L., Taddei, C., Leinse, A., Heideman, R. G., van Dijk, P. W. L., Oldenbeuving, R. M., Marpaung, D. A. I., Burla, M. and Boller, K.-J., "Silicon Nitride microwave photonic circuits," Opt. Express, vol. 21, no. 19, 22937-22961 (2013).

[11] Guzzon, R. S., Norberg, E. J., Parker, J. S., Johanssen, L. A., and Coldren, L. A., "Integrated InP-InGaAsP tunable coupled ring optical bandpass filters with zero insertion loss," Opt. Express, vol. 19, no. 8. 7816-7826 (2011).

[12] Ibrahim, S., Fontaine, N. K., Djordjevic, S. S., Guan, B., Su, T., Cheung, S., Scott, R. P., Pomerene, A. T., Seaford, L. L., Hill, C. M., Danziger, S., Ding, Z., Okamoto, K., and Yoo, S. J. B., "Demonstration of a fast-reconfigurable silicon CMOS optical lattice filter," Opt. Express, vol. 19, no. 14, 13254-13256 (2011).

[13] Doerr, C. R., Stulz, L. W., and Pafchek, R., "Compact and low-loss integrated box-like passband multiplexer," IEEE Photon. Technol. Lett., vol. 15, no. 7, 918-920 (2003).

[14] Oguma, M., Kitoh, T., Mori, A. and Takahashi, H., "Ultrawide-passband tandem MZI-synchronized AWG and group delay ripple balancing out technique," We.8.E.2, ECOC2010, Torino, Italy.

[15] Ishida, O. and Takahashi, H., "Loss-imbalance equalization in arrayed-waveguide-grating (AWG) multiplexer cascades," J. Lightwave Technol., vol. 13, no. 6, 1155-1163 (1995).

[16] Takiguchi, K., Oguma, M., Shibata, T. and Takahashi, H., "Demultiplexer for optical orthogonal frequency-division multiplexing using an optical fast-Fourier-transform circuit," Opt. Lett., vol. 34, no. 12, 1828-1830 (2009).

[17] Goh, T. and Hashizume, Y., "Completely cyclic flat-top optical multi/demultiplexer for multi-carrier transceiver," OTu3C.1, OFC/NEC2013, Anaheim, USA.

[18] Goh, T., Itoh, M., Yamazaki, H., Saida, T., and Hashimoto, T., "Optical Nyquist-Filtering Multi/Demultiplexer with PLC for 1-Tb/s Class Super-Channel Transceiver," Tu3A.5, OFC2015, LA, USA.

[19] Madsen, C. K. & Zhao, J. H. Optical Filter Design and Analysis: A Signal Processing Approach (Wiley, 1999).

[20] Schomogrow, R., Ben-Ezra, S., Schindler, P. C., Nebendahl, B., Koos, C., Freude, W., and Leuthold, J., "Pulse-Shaping with Digital, Electrical, and Optical Filters-A comparison," J. Lightwave Technol., vol. 31, no. 15, 270-2577 (2013).

[21] Sone, K., Wang, X., Oda, S., Nakagawa, G., Aoki, Y., Kim, I., Palacharla, P., Hoshida, T., Sekiya, M., and Rasmussen, J. C., "First Demonstration of Hitless Spectrum Defragmentation using Real-time Coherent Receivers in Flexible Grid Optical Networks," European Conference on Optical Communication 2012 (ECOC2012), Th. 3. D. 1.

[22] Wang, J., Xie, C., and Pan, Z., "Matched Filter Design for RRC Spectrally Shaped Nyquist-WDM Systems," IEEE Photon. Technol. Lett., vol. 25, no. 23, 2263-2266, 2013.

[23] Wang, Z., Chang, S.-J., Ni, C.-Y., and Chen, Y. J., "A high-performance ultracompact optical interleaver based on double-ring assisted Mach-Zehnder interferometer," IEEE Photon. Technol. Lett., vol. 19, no. 14, 1072-1074 (2007).

[24] Luo, L.-W., Ibrahim, S., Nitkowski, A., Ding, Z., Poitras, C. B., Ben Yoo, S. J., and Lipson, M., "High bandwidth on-chip silicon photonic interleaver," Opt. Express, vol. 18, no. 22, 23079-23087 (2010).

[25] Zhuang, L., Beeker, W. P., Leinse, A., Heideman, R., van Dijk, P. W. L., and Roeloffzen, C. G. H., "Novel wideband microwave polarization network using a fully-reconfigurable photonic waveguide interleaver with a two-ring assisted asymmetric Mach-Zehnder Structure," Opt. Express, vol. 21, no. 3, 3114-3124 (2013).

[26] Uranus, H. P., Zhuang, L., Roeloffzen, C. G. H. and Hoekstra, H. J. W. M., "Pulse advancement and delay in an integrated optical two-port ring resonator circuit: direct experiemental observations," Opt. Lett., vol. 32, no. 17, 2620-2622 (2007).

[27] Savory, S. J., "Digital filters for coherent optical receivers," Opt. Express, vol. 16, no. 2, 804-817 (2008).

[28] Zhuang, L., Marpaung, D. A. I., Maurizio, B., Beeker, W. P., Leinse, A., and Roeloffzen, C. G. H., "Low-loss, high-index-contast Si3N4/SiO2 optical waveguides for optical delay lines in microwave photonics signal processing," Opt. Express, vol. 19, no. 23, 23162-23170 (2011).

[29] Wörhoff, K., Heideman, R. G. Leinse, A. & Hoekman, M. TriPleX: a versatile dielectric photonic platform. *Advanced Optical Technol*. **4,** 189-207 (2015).

[30] Johnson, L. M., and Cox, C. H., "Serrodyne optical frequency translation with high sideband suppression," J. Lightwave Technol., vol. 6, no. 1, 109-112 (1988).

[31] Shimizu, S., Cincotti, G. and Wada, N., "Key technologies for energy and spectral efficient flexible optical networks," Proc. of SPIE Vol. 9389, 938903.

[32] Shimizu, S., Cincotti, G. and Wada, N., "Demonstration of no-gurard-interval 6 × 25 Gbit/s all-optical Nyquist WDM system for flexible optical networks by using CS-RZ signal and optical Nyquist filtering," OECC/ACOFT2014, Melbourne, Australia.

[33] Chen Zhu, Bill Corcoran, An Vu Tran, and Arthur J. Lowery, "Nyquist-WDM with Low-Complexity Joint Matched Filtering and Adaptive Equalization", IEEE Photon.Technol. Lett., vol. 26, no. 12, 1211-1214 (2014).

[34] Forney, G. D., "Viterbi Algorithm," Proceedings of The IEEE, vol. 61, no. 3, 268-278 (1973).